Available online at www.sciencedirect.com
ScienceDirect
Journal of Bionic Engineering 13 (2016) 312–323

Analysis of the Vibrissa Parametric Resonance Causing a Signal Amplification during Whisking Behaviour

Tatiana Volkova[1], Igor Zeidis[1], Hartmut Witte[2], Manuela Schmidt[3], Klaus Zimmermann[1]

1. *Technische Universität Ilmenau, Technical Mechanics Group*, 98693 *Max-Planck-Ring* 12, *Ilmenau*, *Germany*
2. *Technische Universität Ilmenau*, *Biomechatronics Group*, 98693 *Max-Planck-Ring* 12, *Ilmenau*, *Germany*
3. *Friedrich-Schiller-Universität Jena*, *Institute of Systematic Zoology and Evolutionary Biology with Phyletic Museum*, 07743 *Erbertstraße* 1, *Jena*, *Germany*

Abstract

The paper deals with the mechanical vibrational motion of vibrissae during natural exploratory behaviour of mammals. The theoretical analysis is based on a mechanical model of a cylindrical beam with circular natural configuration under an applied periodic force at the tip, which corresponds to the surface roughness of an investigated object. The equation of motion of the beam is studied using the Euler-Bernoulli beam theory and asymptotic methods of mechanics. It is shown that from the mechanical point of view the phenomenon of parametric resonance of the vibrissa is possible. It means that the amplitude of forced vibrations of a vibrissa increases exponentially with time, if it is stimulated within a specific resonance frequency range, which depends on biomechanical parameters of the vibrissa. The most intense parametric resonance occurs, when the excitation frequency is close to the doubled natural frequency of free vibrations. Thus, it may be used to distinguish and amplify specific periodic components of a complex roughness profile during texture discrimination.

Keywords: vibrissa, whisking, vibration, tactile sensor, beam theory, parametric resonance

doi: 10.1016/S1672-6529(16)60304-9

1 Introduction

Looking at biologically inspired robotics, it can be stated that the dominating research fields are “locomotion” and “manipulation”. Series of interdisciplinary publications are devoted to locomotion principles, such as walking, swimming, crawling, *etc*.[1–5]. The remarkable exception is biomimetic vibrissal sensing.

In nature, vibrissae are thin long tactile hairs of mammals. They grow usually in groups in different locations on an animal’s body. Mystacial vibrissae, for example, are distributed over a whiskerpad on a snout (Fig. 1a). These whiskers are the most intensely investigated of all vibrissae. Rats, squirrels and other rodents use carpal vibrissae on their legs to get information about the area of putting down the feet (Fig. 1b).

Since quite exactly one hundred years, starting with the famous paper of Vincent[8], who demonstrated the behavioural significance of vibrissae, live scientists and engineers would like to understand their functional principles. Today, one of the motivations for suchlike research on tactile hairs of mammals is that the tactile sensing following biological principles promises to be competitive with artificial vision.

In both cases, whether mystacial or carpal vibrissae, the hairs are levers for transmitting forces and torques that arise at the moment of contact between the hair and an object, to a pressure-sensitive mechanoreceptor–the Follicle-Sinus Complex (FSC). This base of the vibrissa is five-six times larger than the follicle of a regular pelage hair[9]. The FSC consists of a hair follicle and is filled with blood bag called blood-sinus[10] (Fig. 2a). It comprises the follicle, thus ensuring the visco-elastic foundation of the vibrissa. The FSC is embedded in elastic connective tissue and is motile for some groups of vibrissae. This is reflected in anatomical reports that have identified a specialized musculature surrounding the FSC[11,12]. Due to extrinsic and intrinsic muscles, the vibrissae of an animal are repetitively and rapidly moved back and forth (Fig. 2b).

Corresponding author: Tatiana Volkova
E-mail: tatiana.volkova@tu-ilmenau.de

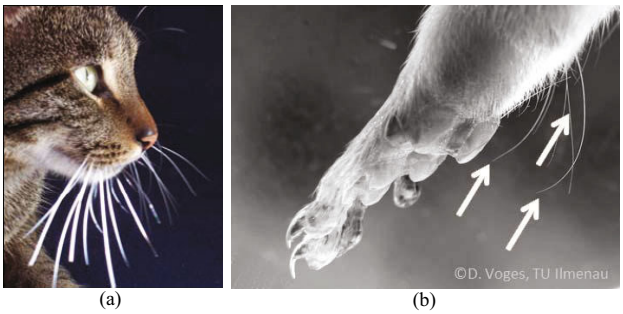

Fig. 1 (a) Mystacial vibrissae of a house cat[6]; (b) Triple of carpal vibrissae (arrows) at a forelimb of Rattus norvegicus[7].

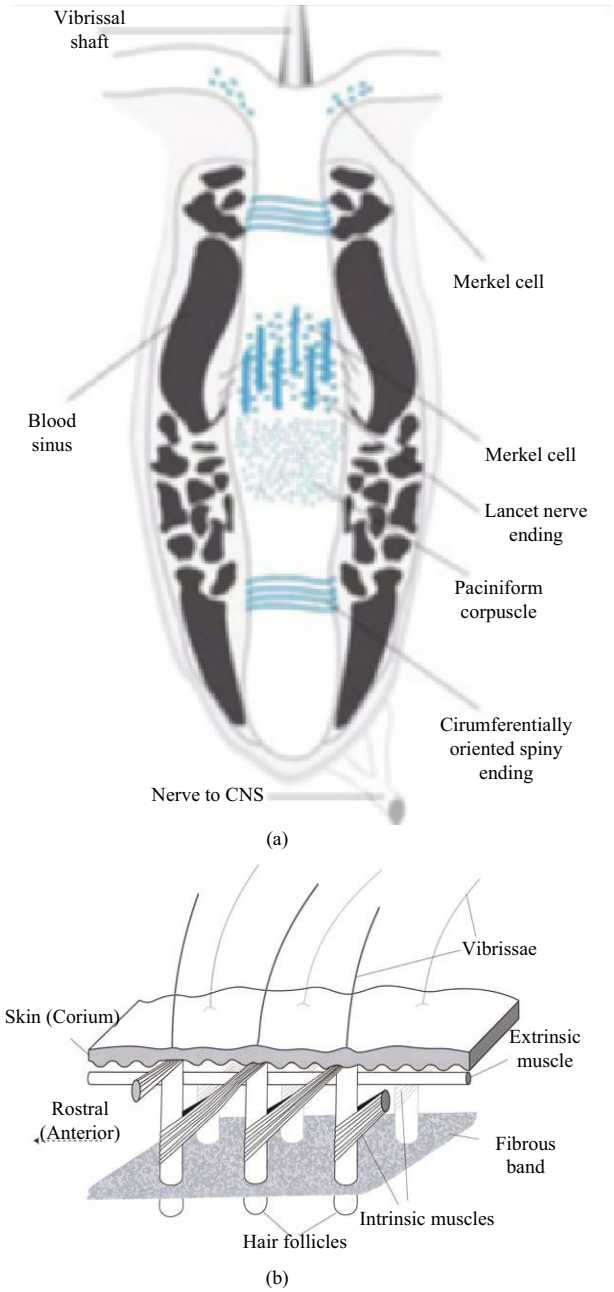

Fig. 2 (a) Structure of the vibrissal FSC anatomy from Refs. [6,10]; (b) Schematic drawing of neighbouring mystacial follicles, which can be moved by extrinsic and intrinsic muscles[11,12].

Mammals use their vibrissae as high-acuity tactile sensors for the exploration of the surrounding area, object localization, and texture discrimination. Rats, for example, can differentiate using mystacial vibrissae rough and smooth surfaces with a groove depth of 30 μm[13]. Since carpal vibrissae are located on the downside aspect of forelimbs, they are probably used as sensors for determining the animal's speed and the duration of stance phase[14]. The ability of mammals to make these fine distinctions prompts that the vibrissa system is made for transmitting high-frequency information. As vibrissal hair has no receptors along its length[10], all the tactile signals at the tip of the vibrissa must be transmitted mechanically to sensory receptors inside the FSC. How vibrissae sense this information, and how it is encoded by the brain, are not known exactly. It is still the focus of many scientific investigations[15].

In publications that describe vibrissa studies, different term sets can be found, for example, "resonance amplification of signals"[16], "vibrissa resonance enhances the sensitivity"[17] or "differential resonance theory"[18]. However, Neimark *et al*.[16] and Hartmann *et al*.[19] confirmed the potential role of vibrissa resonance based on optical measurements of fundamental resonance frequencies of rat vibrissae. The experimental results were analyzed using a theoretical model of the vibrissa as a straight, conical elastic beam, free at the tip and fixed at the base. The same truncated model was taken by Yan *et al*.[20] to obtain numerically fundamental resonance frequencies of the beam under different combinations of boundary conditions (Fig. 3a). The model of the straight vibrissa as a series of discrete nodes contained torsional springs and dampers connected by rigid links with point masses, is presented in Ref. [21]. From the mechanical engineering point of view, however, we lack a general dynamic model of a curved elastic vibrissa sweeping across a surface, which describes its vibrational behaviour during texture discrimination.

In general, resonance is caused by the possibility of a system to store and transfer energy between two or more different storage modes. In case of forced vibrations, when the frequency of an external force is close to a natural frequency of the system, the amplitude of steady-state forced oscillations of the system can reach significant values. This phenomenon is called resonance,

and it is in the focus of the authors mentioned before. Another possibility to excite non-damping vibrations is to change periodically some system parameters to which the system motion is sensitive. A familiar example is a pendulum, whose support is vertically excited. Motion of such systems with one degree of freedom is generally described by an ordinary differential equation

$$\frac{\mathrm{d}^2 x}{\mathrm{d}t^2} + \omega^2(t)\, x = 0, \qquad (1)$$

where the function $\omega(t)$ depends explicitly on time t, and $x(0) \neq 0$. When the amplitude of oscillations caused by the periodic modulation of some parameter increases steadily, the phenomenon of parametric resonance takes place. In contrast to the forced vibrations, parametric resonance may occur not only at discrete frequency values, but also in intervals of frequencies[22]. It can be used to process and amplify even small periodic signals in a physical system or pick out specific frequencies from a complex vibration containing many frequencies.

The present paper deals with this type of resonance phenomenon. We propose a mechanical-mathematical explanation of the vibrissa resonance during texture discrimination. Using a simplified geometry of the curved elastic vibrissa, a model describing in-plane, small vibrations of the beam under a periodic force is developed. Asymptotic methods of mechanics will allow us to draw some analytical conclusions and describe qualitatively the investigated process.

Although the current paper focuses on the vibrissa/beam resonance, strong parallels exist between vibrissa tactile amplification and known mechanisms in auditory encoding. Several resonance properties of the cochlea in the auditory system have a strong frequency selectivity and decompose an auditory signal over resonance frequencies[23,24].

2 Mechanical model of a vibrissa describing parametric resonance

2.1 An overview of the vibrissa modelling

For engineers, the first view on the biological vibrissa leads to the abstraction of a slender rod in a visco-elastic suspension. Therefore, it is no coincidence that former papers on the subject of the vibrissa modelling considered a rigid rod in a pin connection, the movement of which is influenced by springs and dampers[12,25–27]. Behn *et al.*[6,28] improved rigid rod models of vibrissa by the implementation of more complex boundary conditions. They introduced spring and damping elements considering characteristics of the skin and the FSC.

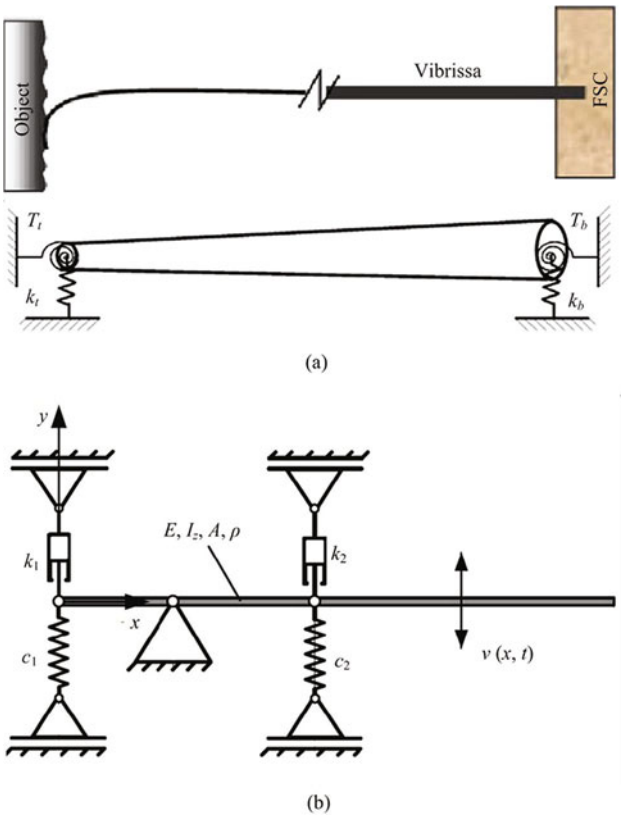

Fig. 3 Continuum beam models of a straight vibrissa with various support conditions from (a) Ref. [20] and (b) Ref. [6].

Continuum models of a vibrissa as an elastic deformable beam following Hooke's law are closer to the biological paradigm, since they are able to take the inherent dynamical behaviour and the bending stiffness of the vibrissa into account[6,20,29,30] (Fig. 3b). Analytical investigations[31] show that it is possible to reconstruct a profile contour by one single quasi-static sweep of the straight elastic beam along the object through calculating the clamping forces and bending moment. In Ref. [32], the forces and bending moment at the vibrissa base during whisking are quantified, paying particular attention to the influence of intrinsic vibrissa curvature.

Since the nineties of the last century, the application of tactile sensors following the functional principles of vibrissae has been in the focus of roboticists[33]. In Refs. [34,35], authors presented ideas and prototypes for artificial tactile hairs or active antennae. In 2005, BIOTACT project team built up biological inspired artificial tactile hairs in the form of glass-fibre rods[36].

A whisker array, where all whiskers move synchronously in one dimension, was used in Ref. [37] for the development of the AMouse mobile robot.

2.2 Assumptions of the model describing parametric resonance

Interaction of a vibrissa with a surface during texture discrimination is a non-linear process. To model it, we need a set of abstractions that enable us to use analytical methods and to describe qualitatively the resonance behaviour of a system.

First assumption concerns the shape of the vibrissal hair. Previous studies show that most of the vibrissae are planar[38]. Therein, vibrissae shape is approximated by a parabola. The results of experimental measurements of the vibrissa diameter at different locations indicate that the diameter evolves linearly along the length of the vibrissa[16,39]. Throughout this paper, the vibrissa is modelled as an Euler-Bernoulli beam whose undeformed neutral axis is an arc of a circle with radius R_0 and central angle $\pi/2-\varphi$ (Fig. 4). The diameter of the beam circular cross-section is assumed to be constant along the axial direction. Herewith, the initial curvature of the beam is constant and equals $\kappa_0 = -1/R_0$.

As the vibrissa sweeps across an object, frictional interactions between the tip and a complex roughness profile generate oscillations of the vibrissa. The arising friction force, like any other function of time, can be decomposed into frequency components with the Fourier transform spectrum. The first several harmonic terms of it may sufficiently reproduce this force function. Thus, in the present model, it is assumed that the roughness profile exerts a time-varying periodic (cosinusoidal) force $\boldsymbol{F}(t)$ that is applied along the beam at the tip (Fig. 4). Its frequency coincides with one of the harmonic components. Results of the behavioural experiments with rats discriminating regular grooved plates are presented in Ref. [40]. In addition, the significance of longitudinal forces occurring during whisking is shown in Refs. [41,42].

The support conditions of the vibrissa inside the FSC are simplified assuming that the beam is pinned at the base. This prevents the deflection of the beam, but allows it to rotate due to the extrinsic and intrinsic muscles (Fig. 2b). The end of the beam is fixed at the right-hand support, which allows horizontal movement along the surface.

It is obvious that the presented mechanical model does not exactly correspond to the describing non-linear process. However, we would like to emphasize that by considering the mentioned assumptions, it is possible to characterize the precurved shape of the biological vibrissa and to derive equations describing its vibrational motion under a periodic force. It would also enable to simplify the equations using analytical methods and to draw some qualitative conclusions.

2.3 Geometry of the model

The right-handed Cartesian coordinate system is placed such that the origin is in the middle of the base's cross-section, and the axial line of the beam lies in the x-y plane, which is the principal plane of the beam at each point (Fig. 4). The circular axial line of the beam can be represented parametrically as $x = R_0(1-\cos(s/R_0))$, and $y = R_0\sin(s/R_0)$, where $s\in[0, L]$ is the natural parameter and $L = R_0(\pi/2-\varphi)$ is the length of the beam.

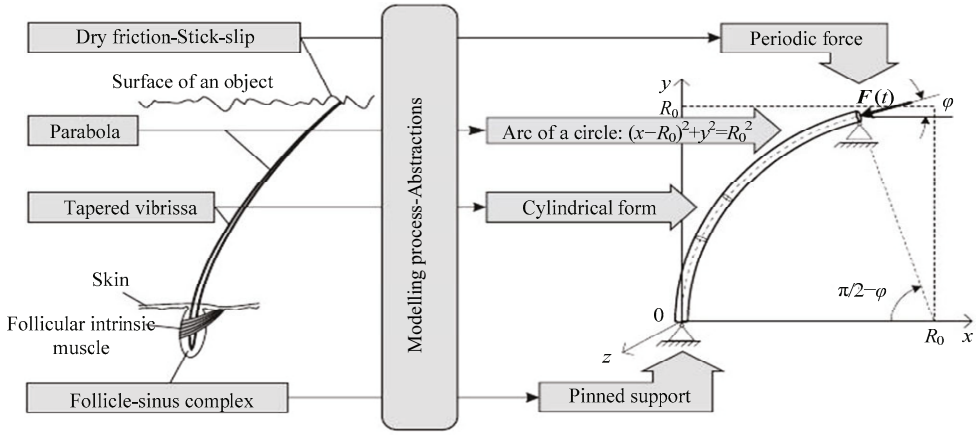

Fig. 4 Assumptions in modelling the process of a vibrissa sweeping past a rough surface.

Consider the orthogonal basis vectors $\boldsymbol{e}_{i0}$, $i = 1, 2, 3$ attached to the axial line of the beam in the static equilibrium configuration, and the orthogonal basis $\boldsymbol{e}_i$, $i = 1, 2, 3$ to the moving curvilinear axial line of the beam (Fig. 5a). Cartesian basis vectors $\boldsymbol{e}_x$, $\boldsymbol{e}_y$, $\boldsymbol{e}_z$ are transformed to the attached basis $\boldsymbol{e}_{i0}$, $i = 1, 2, 3$ by the following matrix:

$$\boldsymbol{L}^0 = \left(\boldsymbol{l}_{ij}^0\right) = \begin{bmatrix} \cos\theta_{30}(s) & \sin\theta_{30}(s) & 0 \\ -\sin\theta_{30}(s) & \cos\theta_{30}(s) & 0 \\ 0 & 0 & 1 \end{bmatrix}, \quad (2)$$

where $\theta_{30}(s) = \pi/2 - s/R_0$ is the angle between the vectors $\boldsymbol{e}_{10}$ and $\boldsymbol{e}_x$ taken positive.

The periodic force $\boldsymbol{F}(t)$ applied directly toward the tip of the beam $s = L$ can be expressed as $\boldsymbol{F}(t) = -F_0\cos(\Omega t)\boldsymbol{e}_1$, where F_0 is the constant amplitude and Ω is the constant angular frequency.

We suppose throughout that the vibrations of the beam caused by the force $\boldsymbol{F}(t)$ about its natural configuration in the x-y plane are small. That means that the displacement vector $\boldsymbol{u}(s, t)$ and the angle $\theta_3(s, t)$ between vectors $\boldsymbol{e}_1$ and $\boldsymbol{e}_{10}$ are of the first order of smallest (Fig. 5a). It is also assumed that φ is a small angle in order to show analytical methods in detail for the slightly simpler case.

Cartesian basis vectors $\boldsymbol{e}_x$, $\boldsymbol{e}_y$, $\boldsymbol{e}_z$ can be transformed to the attached basis $\boldsymbol{e}_i$, $i = 1, 2, 3$ as follows:

$$\boldsymbol{e}_i = \boldsymbol{l}_{ij}\,\boldsymbol{l}_{jk}^0\,\boldsymbol{e}_k\,, \text{where } \boldsymbol{L} = \left(\boldsymbol{l}_{ij}\right) = \begin{bmatrix} 1 & \theta_3(s,t) & 0 \\ -\theta_3(s,t) & 1 & 0 \\ 0 & 0 & 1 \end{bmatrix}. \quad (3)$$

Here, the summation on repeating indexes $j = 1, 2, 3$ and $k = x, y, z$ is meant.

In the attached coordinate system $\boldsymbol{e}_i$, $i = 1, 2, 3$, the displacement vector $\boldsymbol{u}$ of the beam axis points has two time-dependent components:

$$\boldsymbol{u} = u_1(s,t)\,\boldsymbol{e}_1 + u_2(s,t)\,\boldsymbol{e}_2\,. \quad (4)$$

Small deflection theory, together with the assumption of an inextensible axial line, shows that the change in curvature $\Delta\kappa = \kappa - \kappa_0$ and the local transverse displacement $u_2(s, t)$ are related through

$$\Delta\kappa = \kappa_0^2\,u_2 + \frac{\partial^2 u_2}{\partial s^2}, \quad (5)$$

where $\kappa_0 = -1/R_0$. This means that the change in curvature is of first-order smallness.

2.4 Equation of motion

Differential equation that represents the in-plane vibrational motion of a beam is derived from the consideration of the variation of forces and moments across an element of the beam. Consider the free-body diagram of an element of the beam shown in Fig. 5b, where $\boldsymbol{N} = N(s, t)\boldsymbol{e}_1$ is the normal axial force, $\boldsymbol{Q} = Q(s, t)\boldsymbol{e}_2$ is the transverse shear force, and $\boldsymbol{M} = M(s, t)\boldsymbol{e}_3$ is the bending moment.

For the circular beam with constant initial curvature, the in-plane vibrational motion of the beam can be described with a single partial differential equation of sixth order. With regard to the rotary inertia and in the absence of the force of viscous damping, the equation of motion in terms of $u_2(s, t)$ has the following form[43]:

$$\boldsymbol{L}(u_2) = 0, \quad (6)$$

where

$$\begin{aligned} \boldsymbol{L}(u_2) = {} & \rho A\frac{\partial^2 u_2}{\partial t^2} - \frac{\rho A}{\kappa_0^2}\frac{\partial^4 u_2}{\partial s^2\,\partial t^2} \\ & + \rho J\frac{\partial^2}{\partial t^2}\left(\frac{1}{\kappa_0^2}\frac{\partial^4 u_2}{\partial s^4} + 2\frac{\partial^2 u_2}{\partial s^2} + \kappa_0^2 u_2\right) \\ & - EJ\left(\frac{1}{\kappa_0^2}\frac{\partial^6 u_2}{\partial s^6} + 2\frac{\partial^4 u_2}{\partial s^4} + \kappa_0^2\frac{\partial^2 u_2}{\partial s^2}\right) \\ & + \frac{1}{\kappa_0^2}\frac{\partial^2}{\partial s^2}\left(N(s,t)\left(\frac{\partial^2 u_2}{\partial s^2} + \kappa_0^2 u_2\right)\right) \\ & + \frac{1}{\kappa_0}\frac{\partial}{\partial s}\left(Q(s,t)\left(\frac{\partial^2 u_2}{\partial s^2} + \kappa_0^2 u_2\right)\right). \end{aligned}$$

Here, ρ is the mass density of the beam material, $A = \pi d^2/4$ is the cross-sectional area, d is the diameter of the beam, $J = \pi d^4/64$ is the moment of inertia of the cross-section, and E is Young's modulus, which is assumed to be constant along the beam. Although it was shown experimentally that Young's modulus is larger near the vibrissa tip than that near the base[44].

The components of the normal force $\boldsymbol{N} = N(s, t)\boldsymbol{e}_1$ and the shear force $\boldsymbol{Q} = Q(s, t)\boldsymbol{e}_2$ for the small angle φ are

$$\begin{aligned} N(s,t) &= F(t)\left(\sin(\kappa_0 s) - (1+\varphi)\cos(\kappa_0 s)\right), \\ Q(s,t) &= F(t)\left(\cos(\kappa_0 s) + (1+\varphi)\sin(\kappa_0 s)\right). \end{aligned} \quad (7)$$

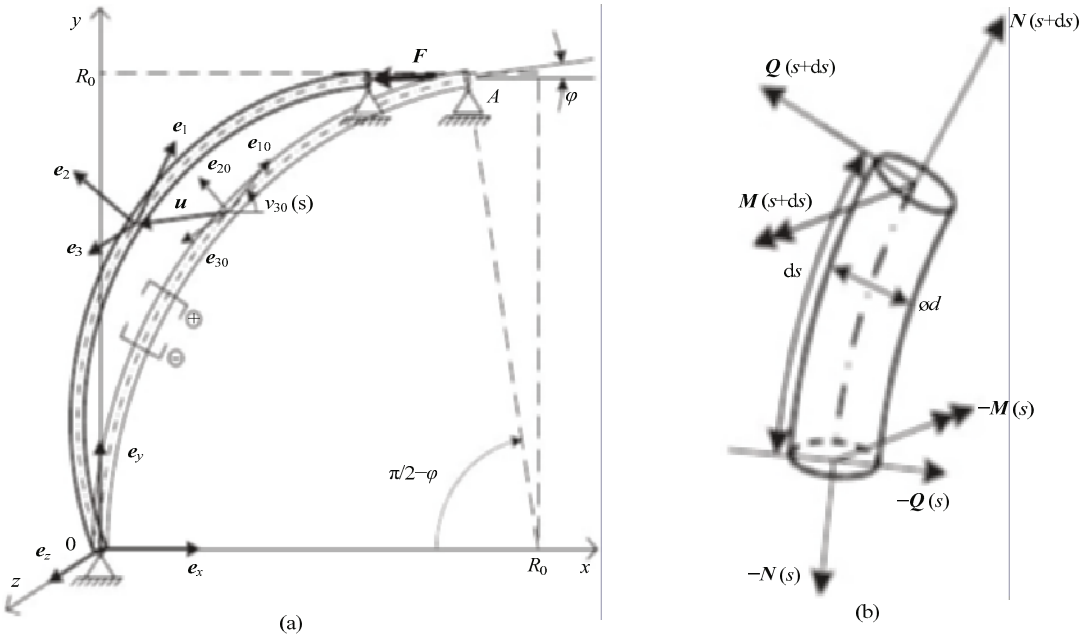

Fig. 5 (a) Deflection of the beam with circular natural configuration under the force acting on the tip of the beam; (b) Free-body diagram of a beam element of infinitesimal length d*s* with internal actions upon it.

The bending moment $\boldsymbol{M} = M(s, t)\boldsymbol{e}_3$ at any cross-section of the beam can be expressed in terms of displacement component $u_2(s, t)$ as

$$M(s,t) = EJ\Delta\kappa = EJ\left(\kappa_0^2 u_2 + \frac{\partial^2 u_2}{\partial s^2}\right). \quad (8)$$

At the pinned left end of the beam $s = 0$, there cannot be any displacements or bending moment. At the right end of the beam the support allows small displacement only in the horizontal direction. That means the y-coordinate of $\boldsymbol{u}$ is zero. Using Eqs. (3) and (4) and retaining linear terms, we get $u_2 = 0$ at $s = L$. Since no external bending moment is applied at the right end of the beam, the bending moment at that location is zero. Consequently, we have the following boundary conditions for the function $u_2(s, t)$ itself as well as for the second derivative of it:

$$u_2(0,t) = u_2(L,t) = 0,$$
$$\left.\frac{\partial^2 u_2(s,t)}{\partial s^2}\right|_{(0,t)} = \left.\frac{\partial^2 u_2(s,t)}{\partial s^2}\right|_{(L,t)} = 0. \quad (9)$$

3 Behaviour of the circular beam near the resonance

3.1 Approximation of the equation of motion

To solve Eq. (6), Galerkin's method is used, that is a method for finding the approximate solution of a differential equation[45]. This powerful method allows to reduce a partial differential equation to an ordinary one. The basic idea of the method of Galerkin is the following. It is required to determine the solution of the equation $\boldsymbol{L}(u_2) = 0$ which satisfies boundary conditions. We shall seek an approximate solution of the equation in the form:

$$\tilde{u}_2(s,t) = \sum_{i=1}^{n} c_i \phi_i(s) f_i(t), \quad (10)$$

where $\phi_i(s)$, $i = 1, ..., n$, is a certain system of chosen basis functions satisfying the boundary conditions, and c_i are undetermined coefficients. Consider the functions $\phi_i(s)$ to be linearly independent. In order that $\tilde{u}_2(s,t)$ be the solution of the equation $\boldsymbol{L}(u_2) = 0$, it is necessary that $\boldsymbol{L}(\tilde{u}_2)$ is identically equal to zero. This requirement is equivalent to the condition of the orthogonality of $\boldsymbol{L}(\tilde{u}_2)$ to all the functions of the system $\phi_i(s)$, $i = 1, ..., n$. Stating these conditions, the linear system of n equations for the determination of the coefficients c_i follows

$$\int_0^L \boldsymbol{L}\left(\sum_{i=1}^{n} c_i \phi_i(s) f_i(t)\right) \phi_i(s)\, \mathrm{d}s = 0, \quad i = 1, \ldots, n. \quad (11)$$

Thus, substituting c_i in the expression for $\tilde{u}_2(s,t)$, the required approximate solution can be obtained.

In this paper, it is assumed a one-term approximation by Galerkin's Method of Eq. (6) in the form $\tilde{u}_2(s,t)=\sin(\pi s/L)f(t)$, which satisfies the support boundary conditions of the beam Eq. (9). Substituting this expression for $\tilde{u}_2(s,t)$ in Eq. (6), we obtain a second-order ordinary differential equation for the function $f(t)$. It can be written in the dimensionless form as

$$\ddot{f}(\tau)+\left(1-\varepsilon\cos(\gamma\tau)\right)f(\tau)=0, \tag{12}$$

where the dimensionless variables are introduced as first-order approximation with respect to the small angle parameter φ:

$$\tau=\frac{t}{t_c},\ \varepsilon=\frac{512R_0^2F_0}{5\pi^2Ed^4}\left(1-\frac{182}{45\pi}\varphi\right),\ \gamma=\Omega t_c, \tag{13}$$

where

$$t_c=\frac{R_0}{6d}\sqrt{\frac{\rho}{E}\left(80R_0^2+9d^2\right)}\left(1-\frac{2\varphi\left(688R_0^2+27d^2\right)}{3\pi\left(80R_0^2+9d^2\right)}\right). \tag{14}$$

Hereinafter, the dot notation is used to represent a time derivative of a function.

The parameters ε and γ, as they are defined by Eq. (13), depend on biomechanical characteristics of the vibrissa and parameters of the periodic applied force caused by the surface roughness of an investigated object. Consider that the amplitude F_0 of the force to be small in comparison with the elastic forces of the beam element, and the value of the angle φ is taken so that ε can be treated as a small positive parameter.

Eq. (12) is a type of general Eq. (1), which describes the parametric resonance phenomenon. It is known as the Mathieu equation. Periodic solutions of Eq. (12) correspond to specific values of the dimensionless parameters ε and γ. Let us further determine the conditions of the parametric resonance, that is, the ranges of the parameters ε and γ, when the beam performs oscillations whose amplitude progressively increases.

3.2 The procedure of averaging and analytical investigations

For the approximate analysis of non-linear oscillating process described by Eq. (12), the method of averaging is used, when the exact differential equation of the motion is replaced by its averaged version[46]. To use this method, it is needed first to reduce Eq. (12) to the standard form by a change of variables. If we put $\varepsilon = 0$ in the Eq. (12), then it describes a simple harmonic vibration with dimensionless natural frequency equal to unity. The general solution is $f(\tau) = a\cos(\tau+\theta)$, where constants a and θ, respectively, represent the amplitude and phase, which are determined from the initial conditions. The solution to the perturbed equation (when $\varepsilon \neq 0$) is sought in the same form, but now a and θ are allowed to vary with τ:

$$f(\tau)=a(\tau)\cos\left(\tau+\theta(\tau)\right). \tag{15}$$

By following Ref. [46], an additional condition on the functions $a(\tau)$ and $\theta(\tau)$ is imposed:

$$\dot{f}(\tau)=-a(\tau)\sin\left(\tau+\theta(\tau)\right). \tag{16}$$

Then it can be shown that the differential Eq. (12) of second order converts to the system of two equations of the first order for $a(\tau)$ and $\theta(\tau)$:

$$\begin{aligned}\dot{a}(\tau)&=-\frac{\varepsilon}{2}a(\tau)\sin(2\psi)\cos(\gamma\tau),\\ \dot{\theta}(\tau)&=-\varepsilon\cos^2(\psi)\cos(\gamma\tau),\end{aligned} \tag{17}$$

where $\psi = \tau+\theta(\tau)$.

It is shown that the most intense parametric resonance and, therefore, maximal energy transfer to the system occur, when the value of the frequency γ is close to the doubled frequency of free vibrations of the beam[22]. Consequently, we can set

$$\gamma=2+\varepsilon\Delta. \tag{18}$$

The system of Eqs. (17) can be written by introducing a new, slowly varying variable $\xi(\tau) = \gamma\tau - 2\psi$ as follows:

$$\begin{aligned}\dot{a}(\tau)&=-\frac{\varepsilon}{2}a(\tau)\sin(2\psi)\cos\left(\xi(\tau)+2\psi\right),\\ \dot{\xi}(\tau)&=\varepsilon\Delta+2\varepsilon\cos^2(\psi)\cos\left(\xi(\tau)+2\psi\right).\end{aligned} \tag{19}$$

Note that these equations are still exact, no averaging has been made yet. Further on, the assumption for the value of the parameter ε is used: $0 < \varepsilon << 1$.

The method of averaging assumes that if $a(\tau)$ and $\xi(\tau)$ are smooth functions of the time such that their derivatives are small terms of order ε, then the values of these functions can be naturally seen as the superposi-

tion of slowly varying part and small rapidly oscillating terms. Considering these terms cause only small oscillations of real function about its mean part, they can be neglected in zero-order approximation. Thus, the right-hand part of the previous system of Eqs. (19) can be averaged on variable ψ over one period:

$$\begin{aligned}\dot{a}_0(\tau)&=\frac{1}{2\pi}\int_0^{2\pi}\dot{a}(\tau)\,\mathrm{d}\psi=\frac{\varepsilon}{4}a_0(\tau)\sin\left(\xi_0(\tau)\right),\\ \dot{\xi}_0(\tau)&=\frac{1}{2\pi}\int_0^{2\pi}\dot{\xi}(\tau)\,\mathrm{d}\psi=\varepsilon\Delta+\frac{\varepsilon}{2}\cos\left(\xi_0(\tau)\right),\end{aligned}\tag{20}$$

where $a_0 = a$ and $\xi_0 = \xi$ are held fixed during the integration.

The system of differential Eqs. (20) is non-linear. However, it may be simplified to a linear system with constant coefficients by defining new variables

$$\begin{aligned}\eta(\tau)&=a_0(\tau)\cos\left(\frac{\xi_0(\tau)}{2}+\frac{\pi}{4}\right)\ \text{and}\\ \zeta(\tau)&=-a_0(\tau)\sin\left(\frac{\xi_0(\tau)}{2}+\frac{\pi}{4}\right).\end{aligned}\tag{21}$$

Substituting $\eta(\tau)$ and $\xi(\tau)$ into Eq. (20) gives

$$\begin{aligned}\dot{\eta}(\tau)&=-\frac{\varepsilon}{4}\eta(\tau)+\frac{\varepsilon\Delta}{2}\zeta(\tau),\\ \dot{\zeta}(\tau)&=-\frac{\varepsilon\Delta}{2}\eta(\tau)+\frac{\varepsilon}{4}\zeta(\tau).\end{aligned}\tag{22}$$

The matrix corresponding to the system of constant coefficient linear differential Eqs. (22) has the following eigenvalues

$$\lambda^2=\frac{\varepsilon^2}{4}\left(\frac{1}{4}-\Delta^2\right).\tag{23}$$

According to Lyapunov stability theory[47], the solution of Eq. (22) is aperiodic and unstable, if there exists an eigenvalue λ with positive real part. Thus, the resonance takes place within the interval

$$|\Delta|<\frac{1}{2}\tag{24}$$

around the frequency dimensionless value $\omega = 2$.

The range of parameters

$$0<\varepsilon\ll 1\ \text{and}\ |\gamma-2|<\frac{\varepsilon}{2}\tag{25}$$

is called the region of the principal parametric resonance. The width of this region is proportional to the parameter ε.

Parametric resonance may also take place at the frequency ranges close to the values of the form $2/n$ for any natural number n. However, the width of these resonance regions gets narrow proportionally to the value ε^n as n increases. That is why, in practice, the cases for n = 1, 2 and 3 (rarely) are usually observed.

4 Simulation results and their interpretation

It is shown theoretically that the principle parametric resonance of the beam occurs for infinite number of excitation frequency values Ω, see Eqs. (13) and (25):

$$2-\frac{\varepsilon}{2}<\Omega t_c<2+\frac{\varepsilon}{2}.\tag{26}$$

The obtained result can be interpreted qualitatively in the context of biological vibrissa. It is known that geometry and material properties of vibrissal hairs vary from one or the other even at the same mammal individual[39,44]. So each vibrissa can be described by the specific values of the parameters ε and t_c according to Eqs. (13) and (14). In our model, the frequency Ω and the amplitude F_0 of the exciting force correspond to the surface structure of an investigated object (Fig. 4). That is why it can be concluded that each vibrissa has certain resonance properties and thereby it could amplify a specific frequency range caused by the roughness profile. Furthermore, as vibrissae vary systematically in length and thickness across the snout of a mammal[48], the vibrissae system may provide a map of frequency sensitivity, allowing to distinguish a range of different textures during whisking behaviour of an animal. These theoretical findings confirm that vibrissa resonance could be used to perform fine texture discriminations as hypothesized in Refs. [16,17,19].

In order to obtain the numerical results, we assign some realistic values of the biomechanical parameters of vibrissae[6,33]. The prototypical vibrissa is generated by fitting an arc of a circle with radius R_0 = 72 mm and central angle 69°, *i.e.* φ = 21°. So, its length is L = 86.7 mm. The averaged diameter is taken as d = 0.12 mm. The elastic modulus and density of the vibrissa are assumed to be in the same range as that reported for rat whiskers: E = 3.34 GPa, ρ = 1.4 mg·mm^{-3}[16,19,39,44]. The value of the amplitude of the friction force caused by surface roughness are taken as $F_0 = 10^{-5}$ N.

Thus, the prototypical vibrissa has the following value of the dimensionless parameter ε calculated according to Eq. (13): $\varepsilon = 0.1255 << 1$. It could amplify a specific resonance frequency range

$$22.33 \text{ Hz} \le \nu \le 23.78 \text{ Hz}, \tag{27}$$

where $\nu = \Omega/(2\pi)$.

Consider the periodic force acts at the tip of the prototypical vibrissa with a frequency $\nu = 23.08$ Hz, that is within the range (Eq. (27)). Then the corresponding value of the dimensionless parameter $\Delta = 0.014$ lies in the region of the principal parametric resonance, see Eq. (24). From the considerations made above, it may be seen that the movement of the system in this case is defined approximately as

$$f(\tau) = a_0(\tau)\cos\left(\tau + \theta(\tau)\right), \tag{28}$$

where $a_0(\tau)$ is the averaged amplitude of oscillations. After obtaining the unstable solution of Eq. (22), $a_0(\tau)$ is defined as:

$$a_0(\tau) = a_0(0)\sqrt{\frac{e^{2\lambda\tau} + e^{-2\lambda\tau} - 4\Delta}{2 - 4\Delta}}, \text{ where } \lambda = \frac{\varepsilon}{2}\sqrt{\frac{1}{4} - \Delta^2}. \tag{29}$$

Here, $a_0(\tau)$ is the initial perturbation. This means that in the parametric resonance the amplitude of oscillations grows exponentially to infinity.

Fig. 6 shows plots of the averaged amplitude ratio $a_0(\tau)/a_0(0)$ for different values of the parameters ε and Δ, which correspond to the region of the principal parametric resonance. Whereas, the usual resonance takes place only for the driving frequency in forced oscillations, and the amplitude of the solution increases linearly.

The exact solution $f(t)$ of the Mathieu Eq. (12) for $\varepsilon = 0.1255$ and $\Delta = 0.014$ is presented in Fig. 7 in dimensional form. As it is seen in the plot, the averaged amplitude $a_0(t)$ obtained from the analytical considerations and described by the Eq. (29) coincides with the amplitude of the exact oscillating solution.

Thus, the parametric resonance can be defined as increasing oscillations of the system near its unstable equilibrium that arise because of the inevitable initial perturbations. It should be noticed that, when the initial values of f and $\dot{f}$ are exactly zero, they remain zero, unlike what happens in usual resonance, in which the solution increases proportionally with time even from initial values of zero.

If the frequency value of the force is outside of the range (Eq. (27)) amplified by the prototypical vibrissa, then the amplitude of oscillations will remain limited in time. For example, a frequency value $\nu = 24.35$ Hz corresponds to a magnitude of $\Delta = 0.8938$, which lies in the region of stability as $\Delta > 1/2$. In this case, both eigenvalues corresponding to the system of Eqs. (22) are purely complex numbers, and the solution of it is described by real periodic functions. Therefore, the averaged dimensionless amplitude $a_0(\tau)$ of oscillations is given by the following formula:

$$a_0(\tau) = a_0(0)\sqrt{\cos^2(\lambda\tau) + \frac{\Delta + 1/2}{\Delta - 1/2}\sin^2(\lambda\tau)}, \quad \lambda = \frac{\varepsilon}{2}\sqrt{\Delta^2 - \frac{1}{4}}. \tag{30}$$

Fig. 8 shows the exact stable solution $f(t)$ of the Mathieu Eq. (12) for $\varepsilon = 0.1255$ and $\Delta = 0.8938$ in dimensional form. This graph resembles the diagram of beat frequency in acoustics.

In the region of the principal parametric resonance (Eq. (25)), the eigenvalues corresponding to the linear system (Eq. (22)) are real and of opposite sign. That means the critical point of Eq. (22) is a saddle and trajectories approach asymptotically the eigenvector associated with the positive eigenvalue. The phase portrait in the variables $a(t)$ and $\xi(t)$, which are obtained from the exact and averaged systems (Eqs. (19) and (20)), is shown in Fig. 9a. The equidistant points with respect to time are marked with circles. This graph has a horizontal asymptote, since the function $\xi(t)$ tends to a limit ξ_{inf} as t approaches infinity. For $\Delta = 0.014$ the value of ξ_{inf} is

$$\xi_{\text{inf}} = \frac{3\pi}{2} - 2\arctan\left(\frac{1}{\Delta}\left(\frac{1}{2} + \sqrt{\frac{1}{4} - \Delta^2}\right)\right) \approx 1.5987. \tag{31}$$

On the other hand, for the stable case the eigenvalues corresponding to the system (Eqs. (22)) are imaginary numbers. Therefore, its critical point is a center and the trajectories of the solution will be ellipses centered at the origin with clockwise motion in the η-ξ plane. A phase portrait in the variables $a(t)$ and $\xi(t)$ for $\varepsilon = 0.1255$ and $\Delta = 0.8938$ is presented in Fig. 9b.

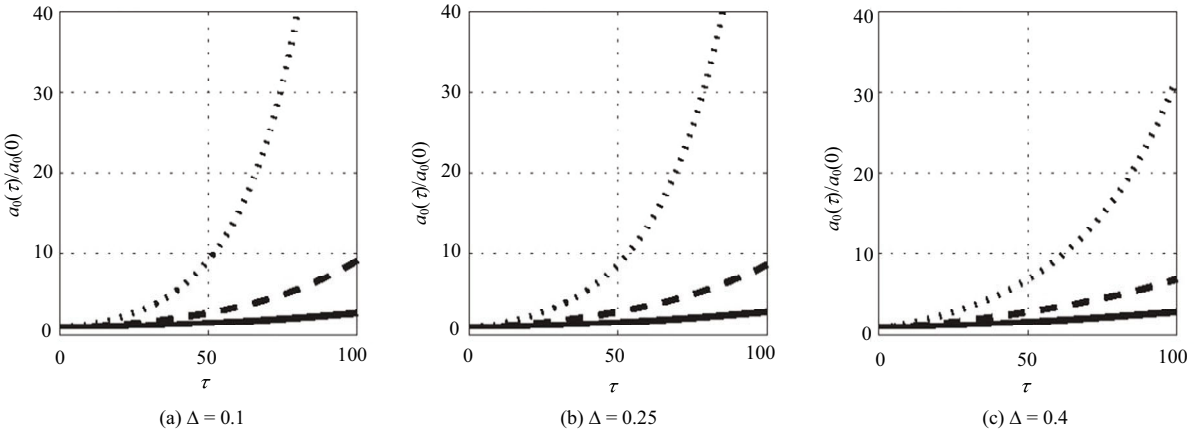

Fig. 6 Amplitude ratio $a_0(\tau)/a_0(0)$ as a function of the time τ obtained by the method of averaging for different values of the parameters ε and Δ, which correspond to the region of the principal parametric resonance: (a) Δ = 0.1; (b) Δ = 0.25; (c) Δ = 0.4. Solid line – ε = 0.05, dashed line – ε = 0.1, dotted line – ε = 0.2.

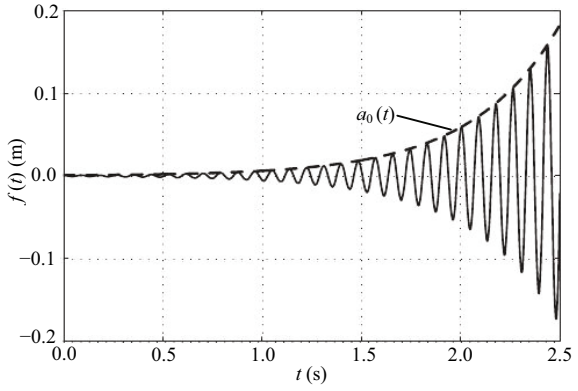

Fig. 7 Solid line corresponds to exact dimensional solution $f(t)$ of the Mathieu Eq. (12) for ε = 0.1255 and Δ = 0.014 in the case of the principle parametric resonance, initial conditions $f(0)$ = 0.0008 m, $\dot{f}(t)=0$ m·s^{-1}; dashed line corresponds to averaged amplitude $a_0(t)$ of the solution described by Eq.(29), $a_0(0)$ = 0.0008 m.

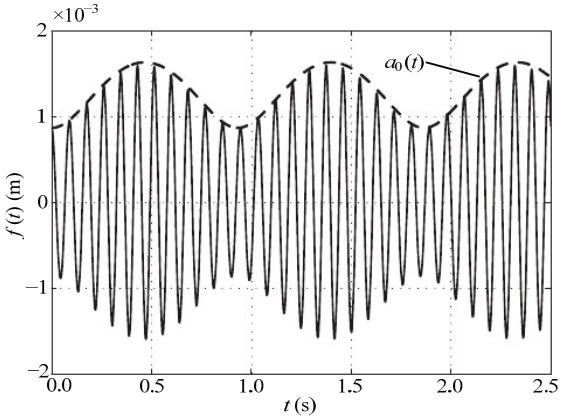

Fig. 8 Solid line corresponds to exact dimensional solution $f(t)$ of the Mathieu Eq. (12) for ε = 0.1255 and Δ = 0.8938, which correspond to the region of stability, initial conditions $f(0)$ = 0.0008 m, $\dot{f}(t)=0$ m·s^{-1}; dashed line corresponds to averaged amplitude $a_0(t)$ of the solution described by Eq. (30), $a_0(0)$ = 0.0008 m.

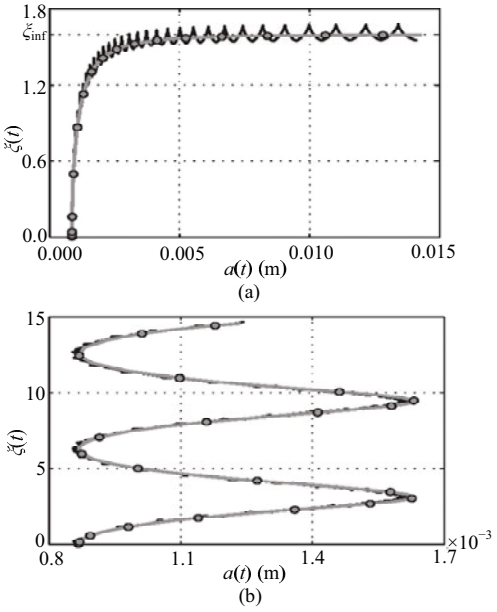

Fig. 9 Phase portrait in the variables $a(t)$ and $\xi(t)$ for ε = 0.1255: (a) Δ = 0.014; (b) Δ = 0.8938. Black line corresponds to the solution of the exact system (Eq. (19)); grey line corresponds to averaged solution of the system (Eq. (20)); circular equidistant marker-points with respect to time on intervals $0 \le t \le 1.4$ s (a) and $0 \le t \le 2$ s (b); initial conditions $a(0)$ = 0.0008 m, $\xi(0)$ = 0.

5 Conclusion

In this paper, a mechanical model of a cylindrical beam with circular natural configuration is developed to study the vibrational motion of mammals' vibrissae during whisking behaviour. The in-plane small oscillations of the beam under a periodic force at the tip, which corresponds to the surface roughness of an investigated object, are modelled using the Euler-Bernoulli beam theory. The approximation of the equation of motion of

the beam is obtained by means of asymptotic methods of mechanics. It is shown theoretically that at specific ranges of the excitation frequency the phenomenon of parametric resonance takes place. It means that the amplitude of forced vibrations of the beam increases exponentially with time, if it is stimulated within a resonance frequency range. The most intense parametric resonance occurs, when the excitation frequency is close to the doubled natural frequency of free vibrations of the beam. The theoretical findings are interpreted qualitatively in the context of biological vibrissa. Since vibrissal hairs are characterized by different values of the biomechanical parameters, each vibrissa has a certain range of the parametric resonance. Thereby, it could distinguish and amplify specific periodic components of a complex roughness profile. This may be particularly important for the detection of objects and texture discrimination during natural exploratory behaviour of mammals. In future work, the model could be improved by considering the tapered shape of the beam, as well as its variable intrinsic curvature that would require numerical methods to solve.

Acknowledgment

This study is supported by the German Research Foundation (DFG) (projects ZI 540-16/2, SCHM 1748/7-2 and WI 1664/4-2). We thank all members of the research team 'Vibrissa' in Jena and Ilmenau (Germany) for the fruitful cooperation. Special thanks go to Joachim Steigenberger for his inspiring ideas and his permanent interest in our work.

References

[1] Tropea C, Bleckmann H (eds.). Nature inspired fluid mechanics. *Notes on Numerical Fluid Mechanics and Multidisciplinary Design*, Springer-Verlag, Berlin Heidelberg, Germany, 2012.

[2] Zimmermann K, Zeidis I, Behn C. *Mechanics of Terrestrial Locomotion*: *With a Focus on Non-pedal Motion Systems*. Springer-Verlag, Berlin Heidelberg, Germany, 2009.

[3] Lepora N, Verschure P, Prescott T. The state of the art in biomimetics. *Bioinspiration & Biomimetics*, 2013, **8**, 1–11.

[4] Wu J, Yang H, Yan S. Energy saving strategies of honeybees in dipping nectar. *Scientific Reports*, 2015, **5**, 15002.

[5] Zhao J, Wu J, Yan S. Erection mechanism of glossal hairs during honeybee feeding. *Journal of Theoretical Biology*, 2015, **386**, 62–68.

[6] Behn C. *Mathematical Modeling and Control of Biologically Inspired Uncertain Motion Systems with Aadaptive Features*. Habilitation thesis, Technische Universität Ilmenau, Germany, 2013.

[7] Schmidt M, Witte H, Zimmermann K, Niederschuh S, Helbig T, Voges D, Husung I, Volkova T, Will C, Behn C, Steigenberger J, Klauer G. Technical, non-visual characterization of substrate contact using carpal vibrissae as a biological model: An overview. *Proceedings of the* 58*th International Scientific Colloquium*, Ilmenau, Germany, 2014.

[8] Vincent S. The function of vibrissae in the behavior of the white rat. *Behavior Monographs*, 1912, **1**, 1–81.

[9] Ahl A. The role of vibrissae in behavior: A status review. *Veterinary Research Communications*, 1986, **10**, 245–268.

[10] Ebara S, Kumamoto K, Matsuura T, Mazurkiewicz J, Rice F. Similarities and differences in the innervation of mystacial vibrissal follicle-sinus complexes in the rat and cat: A confocal microscopic study. *Journal of Comparative Neurology*, 2002, **449**, 103–119.

[11] Dörfl J. The musculature of the mystacial vibrissae of the white mouse. *Journal of Anatomy*, 1982, **135**, 147–154.

[12] Haidarliu S, Simony E, Golomb D, Ahissar E. Muscle architecture in the mystacial pad of the rat. *The Anatomical Record*, 2010, **293**, 1192–1206.

[13] Carvell G, Simons D. Biometric analyses of vibrissal tactile discrimination in the rat. *The Journal of Neuroscience*, 1990, **10**, 2638–2648.

[14] Niederschuh S, Witte H, Schmidt M. The role of vibrissal sensing in forelimb position control during travelling locomotion in the rat (*Rattus norvegicus*, Rodentia). *Zoology*, 2014, **118**, 51–62.

[15] Prescott T, Ahissar E, Izhikevich E (eds.). *Scholarpedia of Touch*, Atlantis Press, Paris, France, 2016.

[16] Neimark M, Andermann M, Hopfield J, Moore C. Vibrissa resonance as a transduction mechanism for tactile encoding. *The Journal of Neuroscience*, 2003, **23**, 6499–6509.

[17] Andermann M, Moore C. Mechanical resonance enhances the sensitivity of the vibrissa sensory system to near-threshold stimuli. *Brain Research*, 2008, **1235**, 74–81.

[18] Jadhav S, Feldman D. Texture coding in the whisker system. *Current Opinion in Neurobiology*, 2010, **20**, 313–318.

[19] Hartmann M, Johnson N, Towal R, Assad C. Mechanical characteristics of rat vibrrissae: Resonant frequencies and damping in isolated whiskers and in the awake behaving animal. *The Journal of Neuroscience*, 2003, **23**, 6510-6519.

[20] Yan W, Kan Q, Kergrene K, Kang G, Feng X, Rajan R. A truncated conical beam model for analysis of the vibration of rat whiskers. *Journal of Biomechanics*, 2013, **46**,

1987–1995.

[21] Quist B, Seghete V, Huet L, Murphey T, Hartmann M. Modeling forces and moments at the base of a rat vibrissa during noncontact whisking and whisking against an object. *The Journal of Neuroscience*, 2014, **34**, 9828–9844.

[22] Landau L, Lifshitz E. Mechanics. *Course of Theoretical Physics*, 2nd ed., Pergamon Press, Oxford, United Kingdom, 1969.

[23] Geisler C. *From Sound to Synapse*, Oxford University Press, New York, USA, 1998.

[24] Warren R. *Auditory Perception*: *An Analysis and Synthesis*, 3rd ed., Cambridge University Press, Cambridge, United Kingdom, 2008.

[25] Berg R, Kleinfeld D. Rhythmic whisking by rat: Retraction as well as protraction of the vibrissae is under active muscular control. *Journal of Neurophysiology*, 2003, **89**, 104–117.

[26] Mitchinson B, Gurney K, Redgrave P, Melhuish C, Pipe A, Pearson M, Gilhespy I, Prescott T. Empirically inspired simulated electro-mechanical model of the rat mystacial follicle-sinus complex. *Proceedings of the Royal Society of London B*: *Biological Sciences*, 2004, **271**, 2509–2516.

[27] Hill D, Bermejo R, Zeigler H, Kleinfeld D. Biomechanics of the vibrissa motor plant in rat: Rhythmic whisking consists of triphasic neuromuscular activity. *The Journal of Neuroscience*, 2008, **28**, 3438–3455.

[28] Behn C, Schmitz T, Witte H, Zimmermann K. Animal vibrissae: modelling and adaptive control of bio-inspired sensors. *Proceedings of the* 12*th International Work-Conference on Artificial Neural Networks*, Tenerife, Spain, 2013, 159–170.

[29] Scholz G, Rahn C. Profile sensing with an actuated whisker. *IEEE Transactions on Robotics and Automation*, 2004, **20**, 124–127.

[30] Schäfer M, Schmitz T, Will C, Behn C. Transversal vibrations of beams with boundary damping in the context of animal vibrissae. *Proceedings of the* 56*th International Scientific Colloquium*, Ilmenau, Germany, 2011.

[31] Will C, Steigenberger J, Behn C. Object contour reconstruction using bio-inspired sensors. *Proceedings of the* 11*th International Conference on Informatics in Control*, *Automation and Robotics*, Vienna, Austria, 2014, 459–467.

[32] Quist B, Hartmann M. Mechanical signals at the base of a rat vibrissa: the effect of intrinsic vibrissa curvature and implications for the tactile exploration. *Journal of Neurophysiology*, 2012, **107**, 2298–2312.

[33] Carl K. *Technische Biologie des Tasthaar-Sinnessystems als Gestaltungsgrundlage für taktile stiftführende Mechanosensoren*. Ph.D. thesis, Technische Universität Ilmenau, Germany, 2009. (in German)

[34] Zimmer U. Self-localization in dynamic environments. *IEEE*/*SOFT International Workshop BIES*'95, Tokio, Japan, 1995.

[35] Kaneko M, Kanayama N, Tsuji T. Vision based active antenna. *IEEE International Conference on Robotics and Automation*, Minneapolis, USA, 1996, **3**, 2555–2560.

[36] Pearson M, Mitchinson B, Sullivan J, Pipe A, Prescott T. Biomimetic vibrissal sensing for robots. *Proceedings of the Royal Society of London B*: *Biological Sciences*, 2011, **366**, 3085–3096.

[37] Fend M, Bovet S, Hafner V. The artificial mouse-A robot with whiskers and vision. 35*th International Symposium on Robotics* , Paris, France, 2004.

[38] Knutsen P, Biess A, Ahissar E. Vibrissal kinematics in 3D: Tight coupling of azimuth, elevation, and torsion across different whisking modes. *Neuron*, 2008, **59**, 35–42.

[39] Voges D, Carl K, Klauer G, Uhlig R, Schilling C, Behn C, Witte H. Structural characterization of the whisker system of the rat. *IEEE Sensors Journal*, 2012, **12**, 332–339.

[40] Zuo Y, Perkon I, Diamond M. Whisking and whisker kinematics during a texture classification task. *Philosophical Transactions of the Royal Society B*, 2011, **366**, 3058–3069.

[41] Gopal V, Hartmann M. Using hardware models to quantify sensory data acquisition across the rat vibrissal array. *Bioinspiration & Biomimetics*, 2007, **2**, S135–S145.

[42] Stüttgen M, Kullmann S, Schwarz C. Responses of rat trigeminal ganglion neurons to longitudinal whisker stimulation. *Journal of Neurophysiology*, 2008, **100**, 1879–1884.

[43] Svetlitsky V. *Dynamics of Rods*, Springer-Verlag, Berlin Heidelberg, Germany, 2005.

[44] Quist B, Faruqi R, Hartmann M. Variation in young's modulus along the length of a rat vibrissa. *Journal of Biomechanics*, 2011, **44**, 2775–2781.

[45] Kantorovich L, Krylov V. *Approximate Methods of Higher Analysis*, Groningen, Netherlands, 1958.

[46] Bogolyubov N, Mitropoliskii Y. *Asymptotic Methods in the Theory of Nonlinear Oscillations*. Gordon and Breach Science Publishers, New York, USA, 1961.

[47] Malkin I. *Theory of Stability of Motion*, United States Atomic Energy Commission, Washington, D.C., USA, 1959.

[48] Brecht M, Preilowski B, Merzenich M. Functional architecture of the mystacial vibrissae. *Behavioural Brain Research*, 1997, **84**, 81–97.